Available online at www.sciencedirect.com
ScienceDirect
International Journal of Heat and Mass Transfer 51 (2008) 3736–3744
International Journal of HEAT and MASS TRANSFER
www.elsevier.com/locate/ijhmt

Three-fluid model predictions of pressure changes in condensing vertical tubes

Vladimir D. Stevanovic [a,*], Miroslav Stanojevic [a], Dejan Radic [a], Milorad Jovanovic [b]

[a] Faculty of Mechanical Engineering, University of Belgrade, Kraljice Marije 16, 11120 Belgrade, Serbia
[b] Thermal Power Plant "Nikola Tesla", 11500 Obrenovac, Serbia

Received 9 October 2007
Available online 4 March 2008

Abstract

Pressure changes in annular downward flows of condensing steam in vertical tubes are predicted with a three-fluid model. Several available correlations for the steam–liquid film interfacial friction are applied in the three-fluid model. Since discrepancies are obtained between calculated and measured pressure changes, a new correlation for the interfacial friction coefficient is proposed by taking into account the influence of the steam and liquid density ratio. The new correlation provides good agreement. The influence of the gravitational, frictional and acceleration pressure changes on the total pressure change is analysed, as well as the droplets entrainment from the liquid film surface to the steam core.

Keywords: Condensation; Pressure change; Three-fluid model

1. Introduction

Steam condensation inside vertical tubes is applied in various heat exchangers in power and chemical industry. Some examples are air heaters in steam boilers [1], air-cooled condensers [2], and steam condensers within the passive systems of nuclear power plants [3]. A typical design of the air heater is depicted in Fig. 1. It consists of rows of condensing tubes in parallel connection from the inlet to the outlet header. Inner wall of the condensing tube is smooth, while the outside is usually finned. An important task in the design of this equipment is to predict the pressure change along the downward flow of condensing steam inside the tube. This pressure change determines the pressure of condensate at the condensing tube outlet and the pressure drop that must be provided in order to remove the drained condensate from the outlet header to the condensate line for its removal. If these conditions are not adjusted, the condensate will accumulate in the lower parts of the condensing tubes, the condensing surface will be reduced, and the freezing of condensate could occur inside tubes of air heaters or air-cooled condensers in cases of low outside air temperatures [1]. In addition, their reliable operation depends on the uniformity of the steam flow distribution between parallel tubes, which can be predicted only based on accurate values of the pressure change along the condensing tube [4].

Measured pressure changes from the inlet to outlet of vertical tubes in which the complete condensation of the downward flowing steam takes place are reported in [4,5]. The measurements were performed in tubes with different inner diameters, spanning from 10 mm to 50 mm, and under pressures in the range from 1 MPa to 7 MPa. An experimental correlation in the form of the Euler number dependence on the steam and liquid density ratio is derived in [4] based on measured data. A separated model of annular flow of liquid film and condensing steam is applied in [5] for the prediction of total inlet to outlet pressure change, where the total pressure change is the sum of the gravitational, acceleration and frictional pressure change terms

* Corresponding author. Tel.: +381 11 3370 561; fax: +381 11 3370 364.
E-mail address: estevavl@eunet.yu (V.D. Stevanovic).

0017-9310/$ - see front matter © 2008 Elsevier Ltd. All rights reserved.
doi:10.1016/j.ijheatmasstransfer.2007.12.008

Nomenclature

A	channel cross-sectional area, m^2
a	interfacial area concentration, m^{-1}
C_D	drag coefficient
D	diameter, m
f	friction coefficient
g	gravitational constant, $m\ s^{-2}$
h	enthalpy, $J\ kg^{-1}$
M	source terms in balance equations
P	pressure, Pa
q_V	volumetric heat flux, $W\ m^{-3}$
Re	Reynolds number
S	perimeter, m
t	time, s
u	velocity, $m\ s^{-1}$
x	coordinate, m
W_d	deposition rate of entrained droplets, $kg\ m^{-2}\ s^{-1}$
W_e	droplets entrainment rate, $kg\ m^{-2}\ s^{-1}$
We	Weber number

Greek symbols

Γ	evaporation/condensation rate, $kg\ m^{-3}\ s^{-1}$
α	volume fraction
δ	liquid film thickness, m
θ	angle of tube inclination, rad
μ	dynamic viscosity, $kg\ m^{-1}\ s^{-1}$
ρ	density, $kg\ m^{-3}$
σ	surface tension, $N\ m^{-1}$
τ	shear stress, $N\ m^{-2}$, relaxation time, s

Subscripts

D	droplet
h	hydraulic parameter
k	phase indicator
0	initial conditions
1	gas
2	liquid film
3	entrained droplets
W	wall

for the steam flow. The steam–liquid film interfacial friction pressure drop is predicted for the smooth liquid film surface. The increase of the steam–liquid film interfacial friction in annular condensing flow due to the mass transfer from the steam core to the surface of the liquid film is investigated in [6]. A semi-theoretical correlation is derived for the interfacial friction coefficient on the liquid film surface, based on the numerical integration of the universal velocity profile in the steam turbulent boundary layer on the smooth liquid film surface. The derived correlation successfully predicts the frictional pressure drops measured in the tube of the flattened cross section [6].

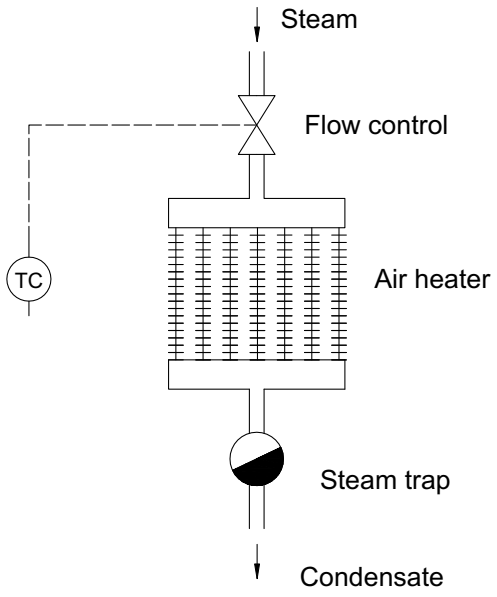

Fig. 1. Typical design of the air heater with steam condensation inside a row of vertical pipes.

In this paper, the three-fluid model is applied as the more general approach for the prediction of the pressure drops in the vertical tubes with condensing steam downward flow. Three-fluid models have been mainly applied for the simulation and analyses of vertical upward annular flows of liquid film, gas phase and entrained droplets under adiabatic or boiling conditions [7–12]. The three-fluid models are based on the mass, momentum and energy balance equations for each of the fluid streams involved in the annular flow. All previous researchers who used the three-fluid models for the annular flow prediction have investigated or at least emphasized the strong dependence of the model results on the correlations for the prediction of mass and momentum interfacial transfers, especially the influence of the correlations for the droplets entrainment and deposition, and liquid film–gas core interfacial friction. In the present work, the ability of the three-fluid model to predict the pressure changes in condensing steam flow in vertical tubes is tested for the available experimental conditions reported in [4,5]. The flow structure and parameters of the annular condensing downward flow are analysed and several available correlations for the interfacial steam–liquid film interfacial friction are tested. The new correlation for the interfacial friction on the wavy liquid film surface is proposed in order to take into account the influence of the steam and liquid density change with pressure on the steam–liquid film interfacial friction. The numerical results obtained with the new correlation show much better agreement with measured data than the previous correlations.

2. Modelling approach

Developed three-fluid model describes annular flow of liquid film, gas core, and droplets that entrain from the

liquid film into the gas core and deposit from the gas core onto the surface of the liquid film, Fig. 2. Mass, momentum and energy balance equations are written for each fluid stream. Transfer processes at the interfaces of fluid pairs that are in contact, as well as between the liquid film and the wall are calculated by the appropriate closure laws.

2.1. Governing equations

The balance equations have the following general form for transient one-dimensional flow conditions

Mass balance

$$\frac{\partial(\alpha_k\rho_k)}{\partial t}+\frac{\partial(\alpha_k\rho_k u_k)}{\partial x}=M_k \tag{1}$$

Momentum balance

$$\frac{\partial(\alpha_k\rho_k u_k)}{\partial t}+\frac{\partial(\alpha_k\rho_k u_k^2)}{\partial x}+\alpha_k\frac{\partial p}{\partial x}=M_{3+k} \tag{2}$$

Energy balance

$$\frac{\partial(\alpha_k\rho_k h_k)}{\partial t}+\frac{\partial(\alpha_k\rho_k h_k u_k)}{\partial x}=M_{6+k} \tag{3}$$

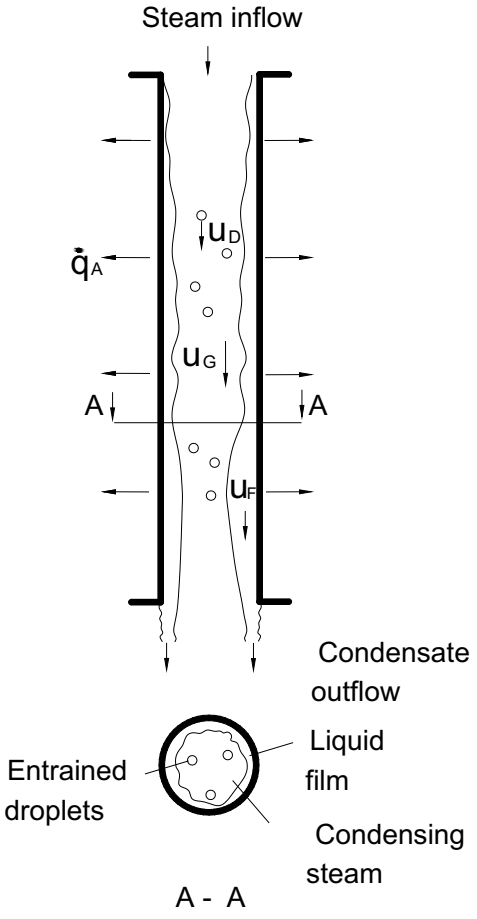

Fig. 2. Fluid streams in condensing vertical pipe.

where M represents mass, momentum and energy source terms as presented in Table 1, and index $k=1$ denotes gas phase, $k=2$ liquid film and $k=3$ entrained droplets. The volume balance is added as

$$\sum_{k=1}^{3}\alpha_k=1 \tag{4}$$

For steady-state conditions ($\partial/\partial t=0$), the above system of balance equations is transformed in a form suitable for the numerical integration as follows. The convection term on the left hand side in Eq. (3) is differentiated, and it is obtained

$$h_k\frac{d(\alpha_k\rho_k u_k)}{dx}+\alpha_k\rho_k u_k\frac{dh_k}{\partial x}=M_{6+k},\quad k=1,2,3 \tag{5}$$

Substituting the mass balance equation (1) into (5) the equation for enthalpy calculation is obtained

$$\frac{dh_k}{dx}=\frac{M_{6+k}-h_kM_k}{\alpha_k\rho_k u_k} \tag{6}$$

Differentiation of the convection term in Eq. (1) and multiplication of Eq. (1) with the fluid velocity gives

Table 1
Source terms in balance Eqs. (1)–(3)

Mass balance source terms

Gas flow

$$M_1=\Gamma_{21}-\Gamma_{12}+\Gamma_{31}-\Gamma_{13} \tag{T1-1}$$

Liquid film

$$M_2=\Gamma_{12}-\Gamma_{21}+\frac{S_{12}}{A}(W_d-W_e) \tag{T1-2}$$

Entrained droplets

$$M_3=\Gamma_{13}-\Gamma_{31}-\frac{S_{12}}{A}(W_d-W_e) \tag{T1-3}$$

Momentum balance source terms

Gas flow

$$M_4=-a_{12}\tau_{12}-a_{13}\tau_{13}+\Gamma_{21}u_2-\Gamma_{12}u_1+\Gamma_{31}u_3-\Gamma_{13}u_1-\alpha_1\rho_1 g\sin\theta \tag{T1-4}$$

Liquid film

$$M_5=a_{12}\tau_{12}-a_{2W}\tau_{2W}+\Gamma_{12}u_1-\Gamma_{21}u_2+\frac{S_{12}}{A}(W_d u_3-W_e u_2)-\alpha_2\rho_2 g\sin\theta \tag{T1-5}$$

Entrained droplets

$$M_6=a_{13}\tau_{13}+\Gamma_{13}u_1-\Gamma_{31}u_3-\frac{S_{12}}{A}(W_d u_3-W_e u_2) \tag{T1-6}$$

Energy balance

Gas flow

$$M_7=(\Gamma_{21}-\Gamma_{12}+\Gamma_{31}-\Gamma_{13})h'' \tag{T1-7}$$

Liquid film

$$M_8=(\Gamma_{12}-\Gamma_{21})h''+\frac{S_{12}}{A}(W_d h_3-W_e h_2)+\dot{q}_{I,2} \tag{T1-8}$$

Line missing

$$\alpha_k \rho_k u_k \frac{du_k}{dx} + \rho_k u_k^2 \frac{d\alpha_k}{dx} + \alpha_k u_k^2 \frac{\partial \rho_k}{\partial p}\frac{dp}{dx} + \alpha_k u_k^2 \frac{\partial \rho_k}{\partial h_k}\frac{dh_k}{dx} = u_k M_k \tag{7}$$

while differentiation of Eq. (2) leads to

$$2\alpha_k \rho_k u_k \frac{du_k}{dx} + \rho_k u_k^2 \frac{d\alpha_k}{dx} + \alpha_k u_k^2 \frac{\partial \rho_k}{\partial p}\frac{dp}{dx} + \alpha_k u_k^2 \frac{\partial \rho_k}{\partial h_k}\frac{dh_k}{dx} + \alpha_k \frac{dp}{dx} = M_{3+k} \tag{8}$$

The velocity derivative is expressed from Eq. (7) as

$$\frac{du_k}{dx} = \frac{u_k M_k - \rho_k u_k^2 \frac{d\alpha_k}{dx} - \alpha_k u_k^2 \frac{\partial \rho_k}{\partial p}\frac{dp}{dx} - \alpha_k u_k^2 \frac{\partial \rho_k}{\partial h_k}\frac{dh_k}{dx}}{\alpha_k \rho_k u_k} \tag{9}$$

Substitution of Eq. (9) in Eq. (8) leads to

$$\frac{d\alpha_k}{dx} = \alpha_k \frac{1 - u_k^2 \frac{\partial \rho_k}{\partial p}}{\rho_k u_k^2}\frac{dp}{dx} - \frac{M_{3+k} - 2u_k M_k + \alpha_k u_k^2 \frac{\partial \rho_k}{\partial h_k}\frac{dh_k}{dx}}{\rho_k u_k^2} \tag{10}$$

Eq. (10) is written for all fluid streams involved in the annular flow pattern, i.e. for $k = 1, 2, 3$, and these equations are summed. Introducing the differential form of Eq. (4)

$$\sum_{k=1}^{3} \frac{d\alpha_k}{dx} = 0 \tag{11}$$

into the sum of Eq. (10) for every fluid, the following equation for the pressure calculation is obtained

$$\frac{dp}{dx} = \frac{\sum_{k=1}^{3} \frac{M_{3+k} - 2u_k M_k + \alpha_k u_k^2 \frac{\partial \rho_k}{\partial h_k}\frac{dh_k}{dx}}{\rho_k u_k^2}}{\sum_{k=1}^{3} \alpha_k \frac{1 - u_k^2 \frac{\partial \rho_k}{\partial p}}{\rho_k u_k^2}} \tag{12}$$

The final set of balance equations is derived in the form of Eqs. (6), (9), (10) and (12). These equations are written for every fluid stream involved in the modeled annular two-phase flow pattern. This form of derived equations is suitable for the direct application of a numerical integration method. In the present work, the Runge–Kutta method is applied. Derivatives of the dependant parameters are calculated in the following order. First, the enthalpy derivative is calculated from Eq. (6). Than, the pressure derivative is calculated from Eq. (12) by using the result of Eq. (6). Eq. (10) is calculated by using the solutions from (6) and (12), and finally, Eq. (9) is calculated by using the results of previous three Eqs. (6), (10) and (12). The numerical procedure represents the solution of the Cauchy problem, where the initial conditions are flow parameters at the inlet of the condensing tube (dependent variables $\alpha_{k,0}$, $u_{k,0}$, $h_{k,0}$, p_0).

2.2. Closure laws

Expressions for the calculation of interfacial areas between the liquid film and the tube inner wall, the liquid film and the gas phase core and between the gas phase and the entrained droplets, per unit volume of the flow channel, are presented in Table 2 (Eqs. (T2-1), (T2-2) and (T2-8)). In the model, the entrained droplets are represented with the mean diameter based on the Weber number (Eqs. (T2-9) and (T2-10)). The wavy liquid film on the tube wall (Fig. 2) is observed in the tube cross section as a ring with the mean thickness δ (Eq. (T2-5)). Hydraulic diameters of the gas phase core and the liquid film stream, necessary for the calculation of the corresponding Reynolds numbers are calculated with Eqs. (T2-6) and (T2-7).

Table 2
Geometric constitutive relations for annular flow

Liquid film-wall interfacial area concentration

$$a_{2W} = \frac{4}{D} \tag{T2-1}$$

Liquid film–gas interfacial area concentration

$$a_{12} = \frac{S_{12}}{A} \tag{T2-2}$$

where the tube flow cross section is

$$A = \frac{\pi D^2}{4} \tag{T2-3}$$

and the liquid film–gas phase perimeter is

$$S_{12} = \pi D\sqrt{1-\alpha_2} \tag{T2-4}$$

Liquid film thickness

$$\delta = 0.5D(1 - \sqrt{1-\alpha_2}) \tag{T2-5}$$

Hydraulic diameter of the gas phase core

$$D_{h,13} = \frac{4(1-\alpha_2)A}{S_{12}} \tag{T2-6}$$

Hydraulic diameter of the liquid film flow

$$D_{h,2} = \frac{4\alpha_2 A}{S_{2w}} = \alpha_2 D \tag{T2-7}$$

Droplets–gas interfacial area concentration

$$a_{13} = 6\frac{\alpha_3}{D_D} \tag{T2-8}$$

Droplet diameter

$$D_D = \begin{cases} 10^{-4} m & Y \leqslant 10^{-4} \\ Y & 10^{-4} < Y < 3\cdot 10^{-3} \\ 3\cdot 10^{-3} & Y \geqslant 3\cdot 10^{-3} \end{cases} \tag{T2-9}$$

where

$$Y = \frac{\sigma We}{\rho_1 (u_1 - u_3)^2} \tag{T2-10}$$

and the Weber number is $We = 0.799$.

Momentum interfacial transfers due to friction in the multi-fluid model are calculated as the products of the corresponding interfacial area concentrations and the interfacial shear stresses (terms $a_{12}\tau_{12}$, $a_{13}\tau_{13}$ and $a_{2W}\tau_{2W}$ in Eqs. (T1-4)–(T1-6)). Interfacial shear stresses are presented in Table 3, where the friction coefficients are expressed in the Fanning form [13]. Modelling investigations of the condensing flows in this paper have shown that the calculated pressure change strongly depends on the type of the correlation applied for the liquid film–gas phase interfacial friction. Therefore, several available correlations are tested, presented with Eqs. (T4-1)–(T4-5) in Table 4, as well as a

Table 3
Closure laws for shear stresses

Wall shear stress

$$\tau_{2W} = f_{2W}\frac{\rho_2 \mid u_2 \mid u_2}{2} \tag{T3-1}$$

where the liquid film-wall interfacial friction coefficient is

$$f_{2W} = \frac{C}{Re_2^n} \tag{T3-2}$$

For turbulent flow (Blasius correlation, [13])
$C = 0.079$, $n = 0.25$, $Re_2 > 1600$.
For laminar flow $C = 16$, $n = 1$, $Re_2 \leqslant 1600$.
Liquid film Reynolds number is

$$Re_2 = \frac{\rho_2 u_2 D_{h,2}}{\mu_2} \tag{T3-3}$$

Liquid film–gas phase shear stress

$$\tau_{12} = f_{12}\frac{\rho_1}{2} \mid u_1 - u_2 \mid (u_1 - u_2) \tag{T3-4}$$

where applied correlations for the liquid film–gas phase friction coefficient f_{12} are presented in Table 4.

Gas phase–droplets shear stress

$$\tau_{13} = \frac{1}{8}C_D\rho_1 \mid u_1 - u_3 \mid (u_1 - u_3) \tag{T3-5}$$

where the drag coefficient is (Clift et al., [14])

$$C_D = \frac{24}{Re_D}(1 + 0.15Re_D^{0.687}) + \frac{0.42}{1 + 4.25\cdot 10^4 Re_D^{-1.16}} \tag{T3-6}$$

and the droplet Reynolds number is

$$Re_D = \frac{\mid u_1 - u_3 \mid D_D\rho_1}{\mu_1} \tag{T3-7}$$

Table 4
Gas phase–liquid film interface friction coefficient

Modified Wallis correlation [15]

$$f_{12} = \frac{0.079}{Re_1^{0.25}}\left(1 + 300\frac{\delta}{D}\right) \tag{T4-1}$$

where the Reynolds number for the gas core flow is

$$Re_1 = \frac{\rho_1 u_1 D_{h,13}}{\mu_1}$$

Alipchenkov et al. correlation [11]

$$f_{12} = \frac{0.25}{(1.82\log Re_1 - 1.64)^2} + 1.5\frac{\delta}{D} \tag{T4-2}$$

where Re_1 is defined as in case of Wallis correlation (T4-1).

Levitan correlation [16]

$$f_{12} = 0.001\left(\frac{\rho_2}{\rho_1}\right)^{0.4}\left(1 + 300\frac{\delta}{D}\right) \tag{T4-3}$$

Henstock and Hanratty correlation [17]

$$f_{12} = f_s\left\{1 + 1400F\left\{1 - \exp\left[-\frac{(1 + 1400F)^{1.5}}{13.2G_0F}\right]\right\}\right\} \tag{T4-4}$$

where

$$f_s = 0.046Re_1^{-0.2}, F = \frac{[(0.707Re_2^{0.5})^{2.5} + (0.0379Re_2^{0.9})^{2.5}]^{0.4}}{Re_1^{0.8}}\frac{\mu_2}{\mu_1}\left(\frac{\rho_1}{\rho_2}\right)^{0.4},$$

$$G_0 = \frac{Dg\rho_2}{f_s\rho_1 u_1^2}, Re_1 = \frac{\alpha_1\rho_1 u_1 D}{\mu_1},$$

and Re_2 is defined with (T3-3).

Groenewald and Kroeger correlation [6]

$$f_{12} = 0.079\left[\frac{C_1}{Re_1^{0.25}} + \frac{C_2}{Re_1^{1.25}}\right] \tag{T4-5}$$

where

$$C_1 = 1.0046 + 1.719\cdot 10^{-3}Re_w - 9.7746\cdot 10^{-6}Re_w^2$$

$$C_2 = 74.3115 + 24.2891Re_w + 1.8515Re_w^2$$

and the suction Reynolds number for a constant heat flux is

$$Re_w = \frac{d_h}{4L}(Re_{1,in} - Re_{1,out})$$

Proposed new correlation

$$f_{12} = \frac{0.079}{Re_1^{0.25}} + 46.35\frac{\delta}{D}\left(\frac{\rho_1}{\rho_2}\right)^{0.8} \tag{T4-6}$$

new one proposed in this paper Eq. (T4-6). The proposed correlation (T4-6) is the sum of the smooth wall friction factor and a quantity due to the liquid film surface roughness, as it was introduced by Alipchenkov et al. [11] in Eq. (T4-2). This second term comprises the gas phase to liquid film density ratio, in a similar form as Levitan [16] introduced the influence of the phases density ration on the interfacial friction. It is shown in the next section that the new correlation provides much better prediction of the pressure changes in the condensing flows at different pressure levels than the previous ones.

Correlations for the prediction of mass interfacial transfer rates are presented in Table 5. Condensation and evaporation rates are calculated with simple empirical relations that take into account the phase-change relaxation times τ_e and τ_c. The rate of entrainment of liquid from the wavy film to the gas core and the deposition rate of droplets from the gas core to the liquid film are calculated with the correlations developed by Sugawara [9]. These entrainment and deposition correlations were also tested by Kawara et al. [18].

3. Results and discussion

Developed three-fluid model is applied to the simulation of steam condensing downward flows in a vertical tube reported by Kreydin et al. [4]. The tube inner diameter is 0.0132 m and the length is 2.93 m. The inlet saturated steam pressure is varied from 1 MPa to 5 MPa, and the complete steam condensation takes place for different inlet steam mass flow rates, i.e different condensing heat fluxes. The cooling heat flux along the condensing tube length is constant. Three-fluid model predictions with different steam–liquid film interfacial correlations are compared with measured pressure differences between condensing tube outlet and inlet. The obtained results are depicted in Fig. 3. As it is shown, the results strongly depend on the

Table 5
Closure laws for interface mass transfers

Condensation rate

$$\Gamma_{1k} = \begin{cases} \frac{\alpha_k \rho_k}{\tau_c} \frac{h' - h_k}{r} & \text{for } h' > h_k, k = 2,3 \\ 0 \quad \text{for } h' \leqslant h_k \end{cases} \qquad \text{(T5-1)}$$

Evaporation rate

$$\Gamma_{k1} = \begin{cases} \frac{\alpha_k \rho_k}{\tau_e} \frac{h_k - h'}{r} & \text{for } h_k > h', k = 2,3 \\ 0 \quad \text{for } h_k \leqslant h' \end{cases} \qquad \text{(T5-2)}$$

Entrainment rate (Sugawara correlation [9])

$$W_e = 1.07 \frac{\tau_{21} \Delta h_{eq}}{\sigma_2} \frac{u_1 \mu_2}{\sigma_2} \left(\frac{\rho_2}{\rho_1}\right)^{0.4} \qquad \text{(T5-3)}$$

where

$$\Delta h_{eq} = \begin{cases} k_s, & Re_1 \geqslant 10^5 \\ k_s[2.136 \log(Re_1) - 9.68], & Re_1 < 10^5 \end{cases}$$

$$k_s = 0.57\delta_2 + 21.73 \cdot 10^3 \delta_2^2 - 38.8 \cdot 10^6 \delta_2^3 + 55.68 \cdot 10^9 \delta_2^4$$

Deposition rate (Sugawara correlation [9])

$$W_d = k_d C \qquad \text{(T5-4)}$$

$$k_d = 9 \cdot 10^{-3} u_1 (C/\rho_1)^{-0.5} Re_1^{-0.2} Sc_1^{-2/3}$$

$$C = \frac{\dot{m}_3}{\dot{m}_1 u_3/(\rho_1 u_1) + \dot{m}_3/\rho_3}$$

applied interfacial friction correlation. Calculations with previously developed correlations for the gas core–liquid film interfacial friction do not provide adequate agreement. An excellent agreement is obtained with the new correlation, Eq. (T4-6), proposed in this paper. The new correlation takes into account the influence of the pressure level, i.e. the ratio of the steam to liquid density on the steam–liquid film interfacial friction.

Fig. 4 shows an excellent agreement of the three-fluid model predictions with the measured differences of outlet and inlet pressures, together with the frictional, gravitational and acceleration pressure changes. These three pressure change components are obtained by summing the momentum balance equations for all three fluid streams (three equations derived from Eq. (2) for $k = 1, 2, 3$, and with the right hand sides represented with Eqs. (T1-4)–(T1-6)). By introducing Eq. (4), the total pressure change per unit length is derived in the following form

$$\frac{dp}{dx} = -a_{2W}\tau_W - \rho g \sin\theta - \frac{d}{dx}\left(\sum_{i=1}^{3} \alpha_k \rho_k u_k^2\right) \qquad (13)$$

where the two-phase flow density is

$$\rho = \sum_{i=1}^{3} \alpha_k \rho_k \qquad (14)$$

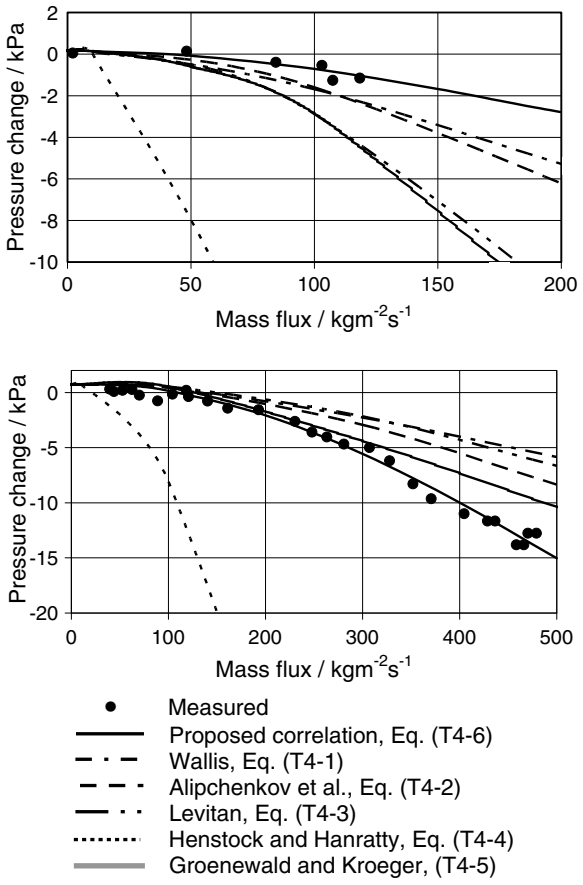

Fig. 3. Comparison of three-fluid model predictions with Kreydin et al. measured data [4], (steam inlet pressure is 1.08 MPa – top, steam inlet pressure is 5 MPa – bottom).

The first term on the right hand side of Eq. (13) represents the frictional pressure drop (i.e. the liquid film friction on the wall), the second represents the gravitational pressure change (for the downward flow in vertical pipe the inclination angle is $\theta = -\pi/2$), and the third term represents the acceleration pressure change. Integration of Eq. (13) provides three pressure change terms presented in Fig. 4. As it is shown, the frictional pressure drop is dominant for mass fluxes higher than 100 kg m^{-2} s^{-1} and the pressure decreases from the tube inlet to outlet. For lower two-phase flow mass fluxes, the pressure increases from the tube inlet to outlet, since the gravitational pressure term is dominant.

Figs. 5 and 6 illustrate the structure of the steam downward condensing flow in vertical tube. The change of the total liquid film and entrained droplets volume fraction along the condensing tube is shown in Fig. 5 for different mass fluxes. This liquid volume fraction reaches values higher than 0.2 only for higher mass fluxes, which also means higher condensing heat fluxes (heat fluxes in cases of 300 kg m^{-2} s^{-1} and 500 kg m^{-2} s^{-1} are respectively -68 W/cm^2 and -112 W/cm^2). The liquid volume fractions below 0.2–0.3 (i.e. steam void above 0.8–0.7) indicate that the annular flow pattern holds along the whole tube length,

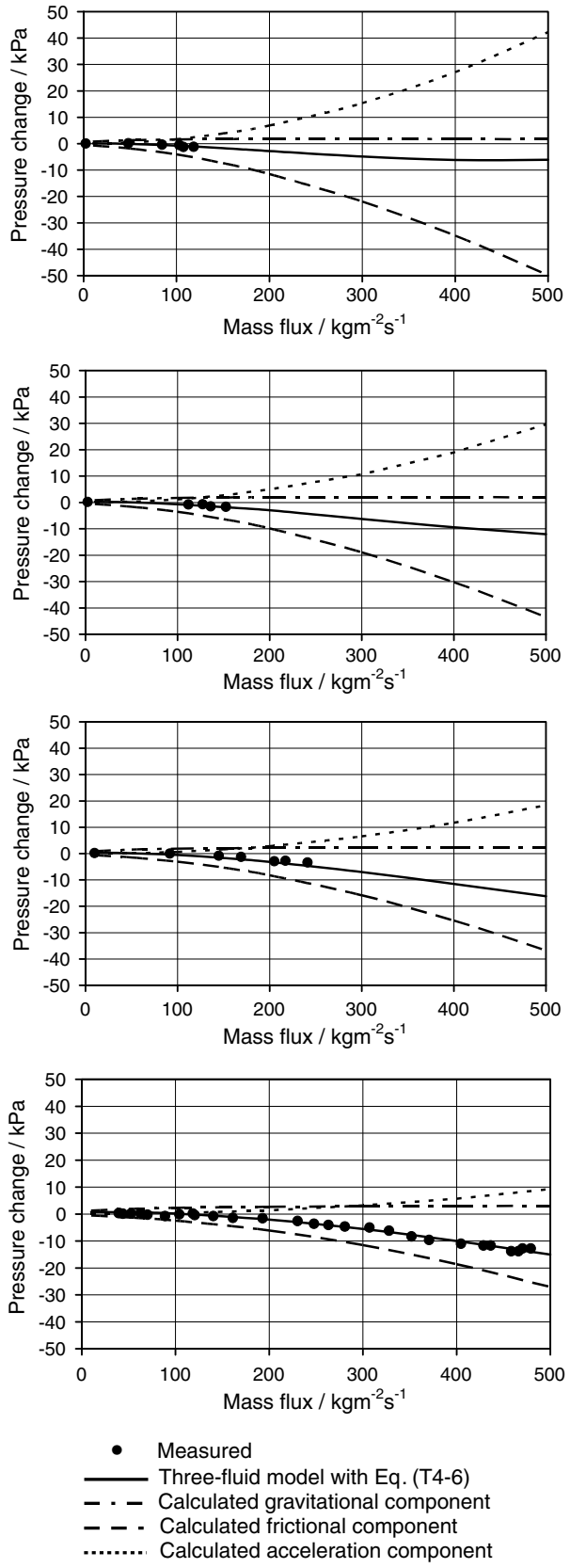

Fig. 4. Comparison of three-fluid model predictions with Kreydin et al. measured data [4] and pressure change components (steam inlet pressure from top to bottom is 1.08 MPa, 1.57 MPa, 2.55 MPa, and 5 MPa).

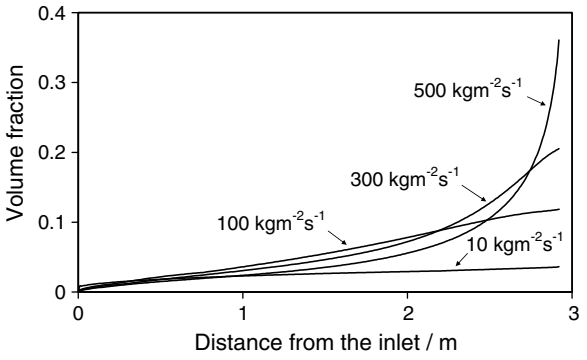

Fig. 5. Condensate volume fraction change from the inlet of vertical condensing tube for different total mass fluxes (steam inlet pressure is 1.08 MPa).

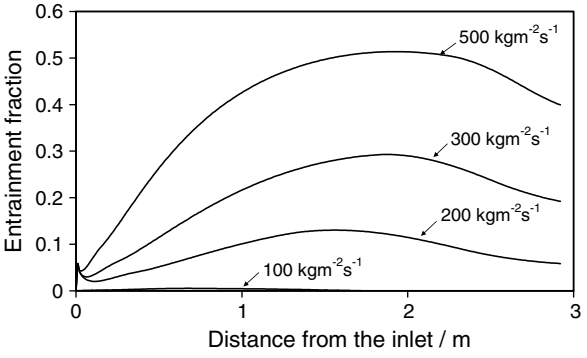

Fig. 6. Fraction of entrained droplets from the inlet of vertical condensing tube for different total mass fluxes (steam inlet pressure is 1.08 MPa).

even for high condensing heat fluxes and corresponding high mass flux rates. The same conclusion is valid for all experimental conditions analysed in this paper, which also justifies the pre-assumption of the annular flow pattern and corresponding application of the three-fluid model. The entrainment fraction in Fig. 6 is calculated as the ratio of droplets mass flow rate, entrained in the steam core, and the total liquid mass flow rate. As expected, the entrainment rate increases with the increase of the total two-phase flow mass flux, i.e. with the increase of the steam velocity.

Developed three-fluid model is also applied to the simulation of steam condensing downward flows in a vertical tube of a larger diameter of 0.0462 m, investigated by Kim and No [5]. The tube length is 1.8 m. The inlet saturated steam pressure is varied from 1 MPa to 7 MPa. The complete steam condensation takes place from tube inlet to outlet. The cooling heat flux along the condensing tube is constant. Calculated pressure differences between outlet and inlet pressures are depicted in Fig. 7 together with the measured values. As shown, very good agreement is obtained. The condensing heat fluxes that correspond to the results in Fig. 7 are depicted in Fig. 8. These heat fluxes are calculated based on the measured condensing steam and tube inner wall temperatures and condensing heat transfer coefficient values presented by Kim and No [5].

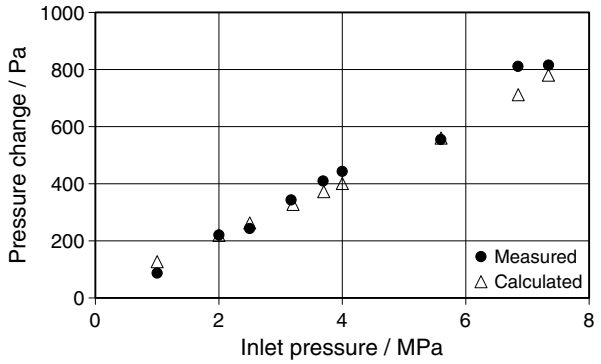

Fig. 7. Comparison of three-fluid model predictions with Kim and No [5] measured data.

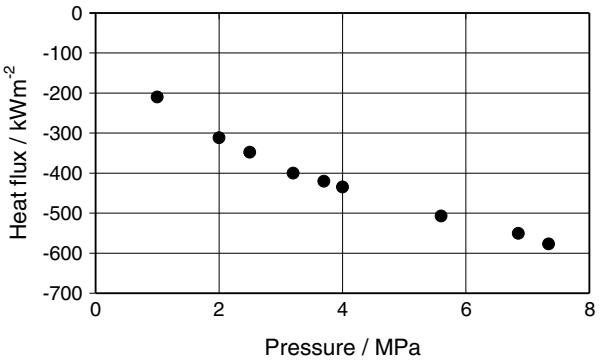

Fig. 8. Heat fluxes at the inner wall of the condensing tube in experimental conditions of Kim and No [5] (input data for three-fluid model calculations presented in Fig. 7).

4. Conclusions

The three-fluid model of condensing downward annular flow in a vertical tube is developed. For steady-state conditions, the model is derived in the form of the system of ordinary differential equations that is solved as the initial value problem by the Runge–Kutta method. Developed model is applied to the simulation and analyses of the available experimental conditions reported in [4,5]. The main findings are:

(a) The calculated pressure changes along the condensing tubes strongly depend on the predictions of the steam–liquid film interfacial friction. Several available correlations for the interfacial friction coefficient are tested, but none of them provides good agreement between calculated and measured pressure change values. Therefore, the new correlation is proposed (Eq. (T4-6), Table 4). Beside liquid film roughness, the new correlation takes into account the influence of the pressure level (i.e. the ratio of the steam and liquid density) on the steam–liquid film interfacial friction. An excellent agreement with measured data is obtained with the new correlation.

(b) Predicted volume fractions show that the annular flow pattern holds even for very high cooling heat fluxes and inlet steam mass fluxes. This justifies the application of the annular flow model for the condensing flows in tubes of heat exchangers, such as air heaters, air-cooled condensers, and condensers within the safety systems of nuclear power plants.

(c) In cases of low condensing steam velocities and corresponding mass flux rates (approximately lower than 100 kg m^{-2} s^{-1} in the pressure range from 1 MPa to 7 MPa), the pressure change along the condensing tube is dominated by the gravitational pressure change and the pressure increases along the downward condensing flow inside the vertical tube. In cases of higher mass fluxes, the frictional pressure drop is dominant and the pressure decreases along the downward condensing flow inside the vertical tube.

(d) The developed three-fluid model is a reliable tool for the prediction of pressure changes in downward condensing steam flows inside vertical tubes of air heaters, air-cooled condensers, and condensers used in nuclear safety systems.

Acknowledgement

This work was partially supported by the Ministry of Science of the Republic of Serbia (Grant 144022).

References

[1] W. Wagner, Water and steam in plants, Vogel Buchverlag, Wuerzburg, 2003 (in German).
[2] D. Butterworth, Condensing equipment, in: G. Hetsroni (Ed.), Handbook of Multiphase Systems, McGraw-Hill, New York, 1982 (Chapter 5.6).
[3] S.H. Chang, H.C. No, W.P. Baek, S.I. Sang, S.W. Lee, Korea looks beyond the next generation, Nucl. Eng. Int. 24 (1997) 553–562.
[4] B.L. Kreydin, I.L. Kreydin, V.A. Lokshin, Experimental research of the total pressure drop in the condensing steam downward flow inside a vertical tube, Therm. Eng. 32 (7) (1985) 42–43 (in Russian).
[5] S.J. Kim, H.C. No, Turbulent film condensation of high pressure steam in a vertical tube, Int. J. Heat Mass Transfer 43 (2000) 4031–4042.
[6] W. Groenewald, D.G. Kroeger, Effect of mass transfer on turbulent friction during condensation inside ducts, Int. J. Heat Mass Transfer 38 (1995) 3385–3392.
[7] T. Saito, D.D. Hughes, M.W. Carbon, Multi-fluid modeling of annular two-phase flow, Nucl. Eng. Des. 50 (1978) 225–271.
[8] S.M. Sami, An improved numerical model for annular two-phase flow with liquid entrainment, Int. Commun. Heat Mass Transfer 15 (1988) 281–292.
[9] S. Sugawara, Droplet deposition and entrainment modelling based on the three-fluid model, Nucl. Eng. Des. 122 (1990) 67–84.
[10] V. Stevanovic, M. Studovic, A simple model for vertical annular and horizontal stratified two-phase flows with liquid entrainment and phase transitions: one-dimensional steady state conditions, Nucl. Eng. Des. 154 (1995) 357–379.
[11] V.M. Alipchenkov, R.I. Nigmatulin, S.L. Soloviev, O.G. Stonik, L.I. Zaichik, Y.A. Zeigarnik, A three-fluid model of two-phase dispersed-annular flow, Int. J. Heat Mass Transfer 47 (2004) 5323–5338.

[12] S.I. Lee, H.C. No, Assessment of an entrainment model in annular-mist flow for a three-field TRAC-M, Nucl. Eng. Des. 237 (2007) 441–450.
[13] F.M. White, Viscous Fluid Flow, McGraw-Hill, New York, 1991, pp. 117, 422.
[14] R. Clift, J.R. Grace, M.E. Weber, Bubbles, Drops and Particles, Academic Press, New York, 1978, p. 111.
[15] G.B. Wallis, One-dimensional Two-phase Flow, McGraw-Hill, New York, 1969.
[16] L.L. Levitan, Dry-out in annular-dispersed flow, Advances in thermal-hydraulics of two-phase flows in energy plants, Science (Nauka), 1987 (in Russian).
[17] W.H. Henstock, T.J. Hanratty, The interfacial drag and the height of the wall layer in annular flows, AICHE J. 22 (1976) 990–1000.
[18] Z. Kawara, I. Kataoka, A. Serizawa, Y.J. Ko, O. Takahashi, Analysis of forced convective CHF based on two-fluid and three-fluid model, in: Proceedings of the 11th International Heat Transfer Conference, 2, 1998, pp. 103–108.